Available online at www.sciencedirect.com
ScienceDirect
Polymer 49 (2008) 943–951
polymer
www.elsevier.com/locate/polymer

Multiwalled carbon nanotubes grafted with polyhedral oligomeric silsesquioxane and its dispersion in poly(L-lactide) matrix

Guang-Xin Chen*, Hiroshi Shimizu

Nanotechnology Research Institute, National Institute of Advanced Industrial Science and Technology, Tsukuba Central 5, 1-1-1 Higashi, Tsukuba, Ibaraki 305-8565, Japan

Received 12 November 2007; received in revised form 28 December 2007; accepted 8 January 2008
Available online 12 January 2008

Abstract

Multiwalled carbon nanotubes (MWNTs) were functionalized with polyhedral oligomeric silsesquioxane (POSS) via amide linkages. The oxidized MWNT (MWNT−COOH) was converted to the acyl chloride-functionalized MWNT (MWNT−COCl) by treating them with thionyl chloride ($SOCl_2$), and then MWNT−COCl was reacted with aminopropylisooctyl-POSS to prepare aminopropylisooctyl polyhedral oligomeric silsesquioxane modified MWNT (MWNT-*g*-POSS). Energy-filtering TEM, FTIR, and Raman spectroscopy revealed that the POSS was covalently attached to the MWNT and the weight gain due to the functionalization was determined by the thermogravimetric analyses (TGA). PLLA/MWNT and PLLA/MWNT-*g*-POSS composites with different MWNT loadings were first prepared by the simple solvent casting approach. A fine dispersion of MWNT-*g*-POSS throughout PLLA matrix was observed by SEM. Moreover, the composites were also prepared by using melt compounding under the different shearing speed of extruder via our custom-built high-shear extruder. A special feedback-type screw was used in this extruder to realize a high shearing flow field. Using this new technique, a uniform dispersion of the neat MWNTs in the PLLA matrix was found under higher screw rotation speed ($\geq$1500 rpm) while poor dispersion was observed under low speed ($<$1500 rpm). The homogeneous dispersion of MWNTs throughout the PLLA/MWNT-*g*-POSS composites without any aggregation was observed at full range of screw rotation speed. The fractured surface of the composites showed not only a uniform dispersion of MWNTs but also a strong interfacial adhesion with the matrix, as evidenced by the presence of many broken but strongly embedded MWNTs in the matrix in the absence of debonding of MWNTs from the matrix. Incorporation of MWNTs improved the mechanical properties.

Keywords: Carbon nanotube; Polyhedral oligomeric silsesquioxane; Poly(L-lactide)

1. Introduction

Carbon nanotubes (CNTs) are considered to be the ideal reinforcing agent for high-strength polymer composites because of their tremendous mechanical strength, nanometer-scale diameter, and high aspect ratio [1]. Studies have shown that carbon nanotubes have ca. 1000 GPa of Young's modulus which is much higher than that of the conventional carbon fibers (200–800 GPa) [2,3]. Despite the advantages of single-walled carbon nanotubes (SWNTs) compared with those of multiwalled ones (MWNTs), a problem associated with the fabrication of polymer composites using SWNTs is that during loading the individual tubes tend to pull out from the ropes (bundles), thus making load transfer difficult. Therefore, the composite reinforcement is dominated by the collective behavior of the bundles rather than by the strength of the individual tubules [4–6]. As far as the MWNTs are concerned, it is noteworthy that MWNTs produced using the arc-discharge method are highly crystalline and defect-free, and the surface is inert so that polymers cannot attach firmly to it. Thus, the introduction of defects via oxidation routes using strong acids or the use of pyrolytically carbon-grown nanotubes (containing defects and kinks) may be an alternative to fabricate composites in which the tube surface is strongly bonded to the polymeric matrix [7]. It has been confirmed that refluxing

* Corresponding author. Fax: +81 29 861 6299.
E-mail address: g.chen@aist.go.jp (G.-X. Chen).

0032-3861/$ - see front matter © 2008 Elsevier Ltd. All rights reserved.
doi:10.1016/j.polymer.2008.01.014

CNTs with concentrated nitric acid creates acidic sites on CNTs, such as carboxylic, carbonyl, and hydroxyl groups [8–10]. These reactive groups on CNTs greatly enhance the combination of CNTs with polymer matrix, thus improving the mechanical strength of the nanocomposites [11]. Sidewall functionalization of CNTs with organic chains or functional groups is another efficient way to improve the dispersion and strengthen the combination of CNTs with polymer matrix [12,13].

After introducing carboxylic acid groups using a nitric acid oxidation method [14–18], the long alkyl chains, polymers, and sugars can be chemically attached to the CNT by esterification and amidation reactions via the carboxylic acid moieties [12,14,19–25]. Tour et al. prepared polystyrene composites with functionalized CNT through the in situ generation of diazonium compounds [12]. Sun et al. functionalized the CNT with poly(vinyl alcohol) and made the functionalized CNT soluble in highly polar solvents [19]. Haddon et al. used carboxylic acid groups to introduce long alkyl chains to CNT via amide linkages or carboxylate–ammonium salt ionic interactions [14]. Sun et al. successfully anchored poly(styrene-*co*-*p*-(4-(4′-vinylphenyl)-3-oxabutanol)) to the CNT via ester linkages [20].

Polyhedral oligomeric silsesquioxane (POSS) reagents, monomers, and polymers are emerging as a new chemical technology for the nano-reinforced organic–inorganic hybrids [26–32] and the polymers incorporating POSS monomers are becoming the focus of many studies due to the simplicity in processing and the excellent mechanical properties, thermal stability and flame retardation etc. [27–37]. The recent development of several families of functional hybrid reagents based on POSS affords a tremendous potential for the modification of organic–inorganic hybrid polymers. The typical POSS monomers possess the structure of cube-octameric frameworks with eight organic corner groups, one or more of which is reactive or polymerizable (Scheme 1). The excellent properties of POSS macromonomer and POSS-containing polymers inspires to prepare the functionalized POSS cages, which can be used as the modification agents of CNTs to prepare the nanocomposites combining the two types of nanoreinforcement agents.

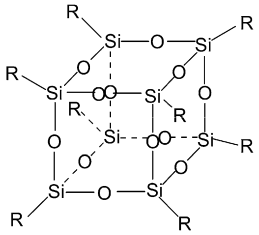

Scheme 1. Structure of polyhedral oligomeric silsesquioxane (POSS).

In this work, we mainly present the synthesis and characterization of aminopropylisooctyl polyhedral oligomeric silsesquioxane modified MWNTs (MWNT-*g*-POSS) as shown in Scheme 2, and subsequently the MWNT-*g*-POSS was employed to prepare the nanocomposites of PLLA. The morphology and thermal properties are addressed based on transmission electronic microscopy (TEM), differential scanning calorimetry (DSC), and thermogravimetric analysis (TGA).

2. Experimental section

2.1. Materials

The multiwalled carbon nanotubes (MWNTs) were provided by Aldrich. The MWNTs were obtained by chemical vapor deposition and the purity was >95%. The outer diameter and inner diameter of MWNTs are 10–20 nm and 5–10 nm, respectively. The starting oxidation temperature of MWNTs is 552.8 °C measured by TGA under an air atmosphere. The Bulk density of MWNTs is 2.1 g/cm^3. Aminopropylisooctyl-POSS was purchased from Hybrid Plastics, and used without further purification. The poly(L-lactide) (PLLA) with a molecular weight of 1.7×10^5 g/mol and a 1.2% D-lactide content used was commercially obtained, which was dried in a vacuum oven at 80 °C for 24 h before processing.

2.2. Purification of MWNT

To remove the impurities such as metallic catalysts in the MWNT, it was treated with 3 M HNO_3 and 1 M H_2SO_4 at 60 °C for 12 h, followed by a reflux process in 5 M HCl at 120 °C for 6 h. The purity of the acid-treated MWNT was measured to be 99% by using the thermogravimetric analysis. These acid-treatments shorten the length of MWNT and introduce carboxyl and hydroxyl groups to MWNT (MWNT–COOH).

2.3. Functionalization of MWNT

The acid-treated MWNT (MWNT–COOH) was reacted with excess $SOCl_2$ for 24 h under reflux, and then the residual $SOCl_2$ was removed by the reduced pressure distillation, to yield acyl chloride-functionalized MWNT (MWNT–COCl). The MWNT–COCl was added into chloroform and the mixture was sonicated for 20 min to create a homogeneous dispersion. The mixture was added with the aminopropylisooctyl-POSS under nitrogen, and then the reactor was immersed in an oil bath at 70 °C under mechanical stirring for 72 h (Scheme 2). The resulting reaction medium was vacuum-filtered through

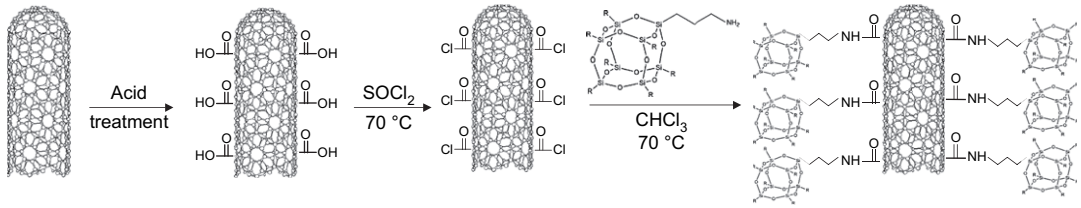

Scheme 2. Illustration for the functionalization of the MWNT with POSS.

a 0.22 μm polycarbonate membrane and washed three times using excess chloroform to yield pure MWNT-*g*-POSS hybrid.

2.4. Dispersion of MWNT-g-POSS in chloroform and PLLA

In order to check the wetting of MWNT-*g*-POSS in organic solvent, such as chloroform, it was dispersed in chloroform and wait for 1 month. MWNT/PLLA composites were prepared in two kinds of methods, namely solution blended and melt compounding. The former one uses chloroform as the co-solvent and the later one uses melting blended of PLLA with the MWNT and MWNT-*g*-POSS, respectively, under different screw rotation speed. The mixture was melt compounded using a custom-built ultrahigh-shear extruder [38] at 190 °C for 4 min. The L/D ratio of the screw was about 1.78. The rotation speed used in this study was from 100 to 2000 rpm. The sample feeds to the top of the screw then returns to the root of the screw through the feedback path. The chamber capability is about 5 ml. The resulting sheet like product was extruded from a T-die. To prevent thermal degradation, a water-cooling system was used around the chamber wall. No apparent degradation resulting from the viscosity of the obtained composites occurred when the rotation speed was lower than 1000 rpm. The dried pellets were then hot pressed at 190 °C for 1 min under 4 atm to prepare the sheets with a thickness of approximately 0.3 mm to use for the various characterizations.

2.5. Measurements

An LEO922 in-column-type energy-filtering transmission electron microscope with a LaB6 cathode equipped with an omega-type energy spectrometer was used at an accelerating voltage of 200 keV to determine the grafting of POSS on MWNT surface. The detailed instrumental setup was described in the previous paper [39]. Silicon elemental maps were created by ''two-window jump ratio'' method, selecting and using two recorded images among those acquired by image-EELS, where the energy-filtered image beyond the silicon ionization edge at around 103 eV (post-edge image) was divided by the energy-filtered image below the ionization edge (pre-edge image). The energy position and the energy width of the two images used for the calculation of the elemental map should be determined to obtain an elemental map with a high S/N ratio.

Fourier-transform infrared (FTIR) spectra were measured at a 2 cm^{-1} resolution using a Digilab FTS 6000ec FTIR spectrophotometer.

The morphology of the composites was observed with a scanning electron microscope (SEM, Hitachi S-4300) at an accelerating voltage of 8 kV after precoating the sample with a homogenous gold layer by ion sputtering.

Raman spectra were measured with a laser Raman microscope (JASCO NRS-2100) using a 514.5 nm Ar line as the excitation source. The laser power was 0.5 W. The spectra were measured in a backscattering configuration with a triple monochromator at intervals of 1 cm^{-1}. The spatial resolution of the microscope was about 2 μm.

The glass transition temperature (T_g) and the melting temperature (T_m) of samples were determined from a Perkin–Elmer DSC 7. The sample sizes ranged from 4 to 6 mg and the T_g and T_m values were obtained from the second melting curves recorded from −30 to 250 °C, scanned at a heating rate of 20 °C/min.

Tensile specimens were prepared from the hot pressed sheets then punched with a dumbbell shaped mold. The specimens were subjected to uniaxial elongation at room temperature. All the experiments were carried out with a Tensilon UMT-300 (Orientec Co. Ltd.) with a cross-head speed of 10 mm/min at 20 °C and 50% relative humidity.

3. Results and discussion

Fig. 1 shows FTIR spectra of MWNT, MWNT-*g*-POSS, and POSS. Comparing with Fig. 1a, in Fig. 1b, the broad band at 1706 cm^{-1} corresponds to the stretching vibration of the C═O group of the amide functionality [40]. The broad and slightly less intense band at 1555 cm^{-1} is assigned to the combination of the bending vibration of the N–H bond and the stretching vibration of the C–N bond of the amide group. In addition, the signal of symmetrical Si–O–Si bonds in the silsesquioxane cages shown in the MWNT-*g*-POSS was characterized by the stretching bands at 1111 cm^{-1}. These FTIR results verify the existence of aminopropylisooctyl-POSS molecules grafted to the MWNTs through the amide bonds.

Fig. 2 shows the TEM images of the MWNT-*g*-POSS after three times of washing with chloroform under sonication to remove the unbound POSS completely. In the TEM images of

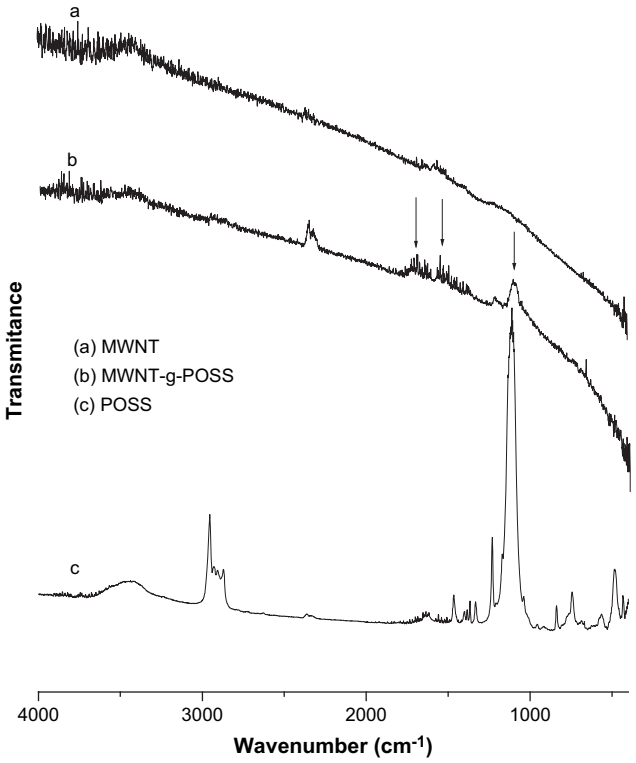

Fig. 1. FTIR spectra of (a) MWNT, (b) MWNT-*g*-POSS, and (c) POSS.

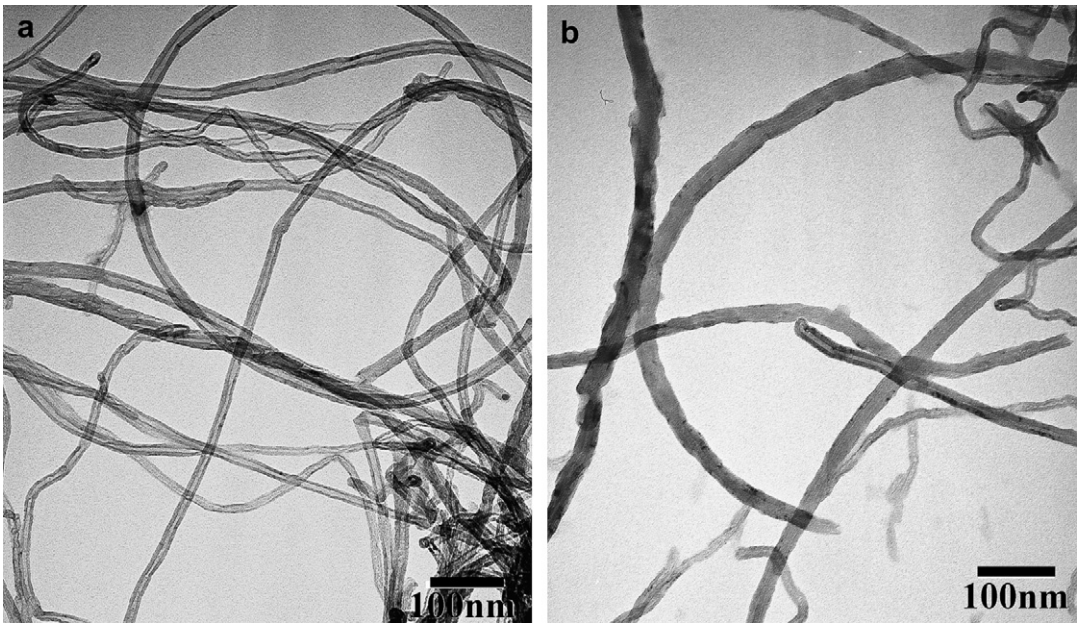

Fig. 2. TEM images of (a) MWNT and (b) MWNT-*g*-POSS.

the neat MWNT (Fig. 2a), the individual tubes were obviously separated from each other. The MWNT wall is relatively smooth and clean and does not appear covered with any extra phase. In contrast, the MWNT-*g*-POSS shown in Fig. 2b appears stained with an extra phase that is presumed to mainly come from the grafted POSS molecules. This indicates that the grafting reaction takes place not only at the tips but also on the whole MWNT surfaces.

More evidence for the MWNT-*g*-POSS was obtained by energy-filtered TEM shown in Fig. 3. Fig. 3a shows a zero-loss image of the MWNT-*g*-POSS, which was formed by the unscattered and elastically scattered electrons with an energy range of 0 ± 10 eV. Image-EELS was performed in the energy ranges that included the silicon L2,3-ionization edges at around 103 eV (Fig. 3b). Fig. 3b shows the silicon distribution images created by the three-window method, where the three appropriate energy-loss positions for the mapping were selected. As expected, the silicon distribution image (Fig. 3b) corresponds to the POSS molecules bounded on the MWNT surface, which shows that elemental silicon was not detected from the neat MWNT surface. In other words, the energy-filtered TEM images show the direct evidence that POSS was grafted onto the MWNT surface.

The amount of the POSS grafted to the MWNT was determined through the TGA analysis under a nitrogen atmosphere. The MWNT-*g*-POSS exhibited a weight loss of about 12 wt% when the temperature is up to 800 °C due to the degradation of the alkyl of grafted POSS on the MWNT, as shown in Fig. 4. The amount of the POSS bound to the MWNT was calculated as 16 wt%.

The Raman spectra shown in Fig. 5 reveal the D- and G-bands of the MWNT at 1350 and 1584 cm^{-1} for both

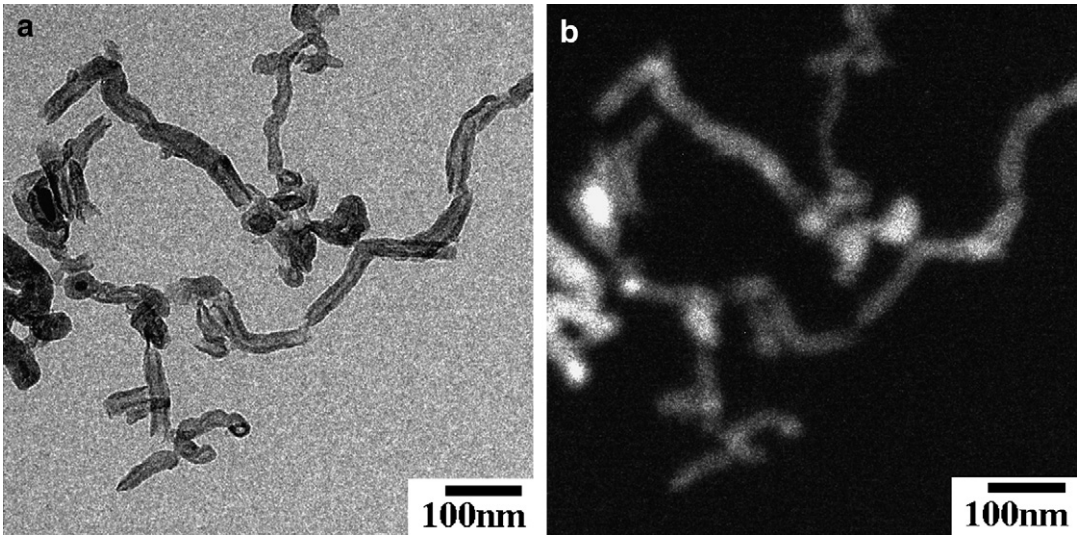

Fig. 3. Electron spectroscopic imaging of MWNT-*g*-POSS. (a) Zero-loss filtered image and (b) silicon distribution images.

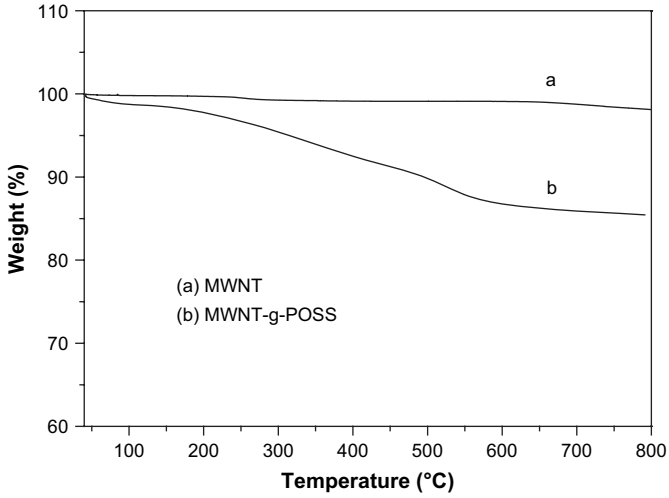

Fig. 4. TGA traces of (a) MWNT and (b) MWN-*g*-POSS.

MWNT and MWNT-*g*-POSS, which were attributed to the defects and disorder-induced peaks and tangential-mode peaks [41]. These are the same as in the pristine nanotubes, which reveals that the electronic structure of the MWNTs remains essentially unperturbed after the incorporation of organic molecules. However, a smooth shoulder band located at 1622 cm^{-1} can be observed for MWNT-*g*-POSS (Fig. 5b). This peak has been related to the sp^2 hybridization of carbon and is used as an evidence of the disruption of the aromatic system of p electrons by the attached molecules [42,43]. The obvious shoulder peak at 1622 cm^{-1} of the MWNT-*g*-POSS samples as compared to the MWNT samples demonstrates a significant content of organic molecules covalently attached.

The functionalized CNTs usually show a much higher solubility or better dispersion in solvents. For example, a stable dispersion was obtained in the case of the MWNT-*g*-POSS when equal amounts of MWNTs were added to the same volume of chloroform, the good solvent of POSS, and mechanically mixed (Fig. 6). As shown in Fig. 6a, all of nanotubes sank in the case of neat MWNTs. This indicates that MWNT-*g*-POSSs (Fig. 6b) possess a higher degree of miscibility than MWNTs due to

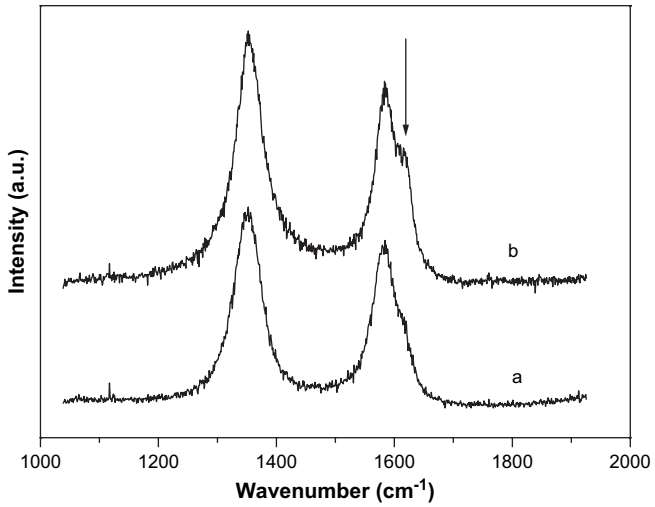

Fig. 5. Raman spectra of (a) MWNT and (b) MWN-*g*-POSS.

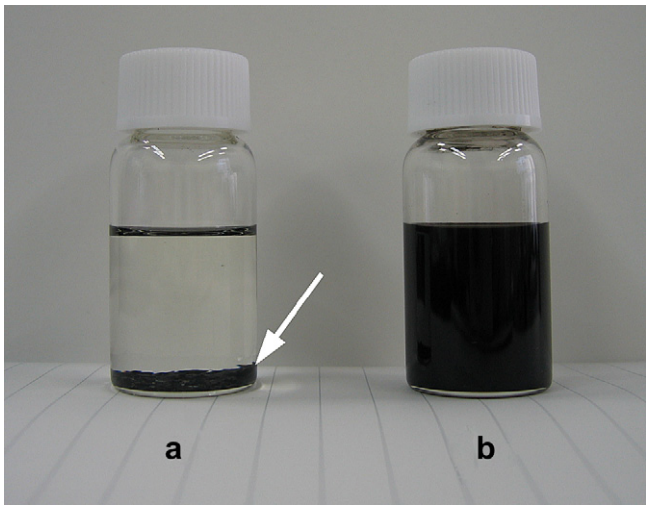

Fig. 6. Photograph of (a) MWNT and (b) MWN-*g*-POSS dispersed in chloroform and wait for 1 month.

the presence of POSS functional groups on the surface, as already proved above. Similar behavior has been observed in the case of polymer functionalized CNTs [44].

Cross-sections of the composites prepared from solvent casting method were made by fracturing the composites in liquid nitrogen to produce an intact fractured surface morphology,

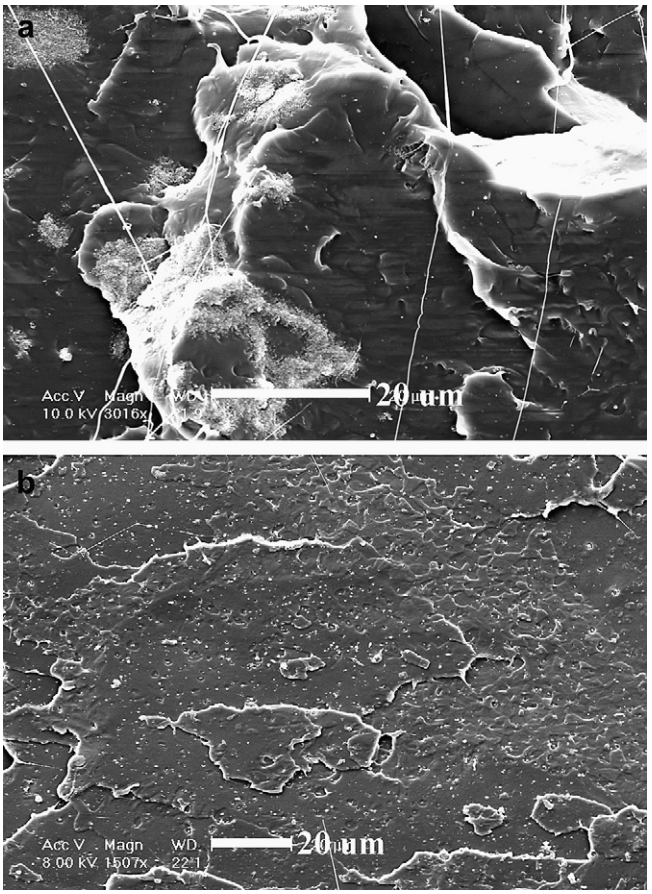

Fig. 7. SEM images of PLLA composites prepared via solvent casting by chloroform (a) PLLA/MWNT with sonicating 30 min, (b) PLLA/MWNT-*g*-POSS without sonication. The content of the MWNTs was 1% by weight.

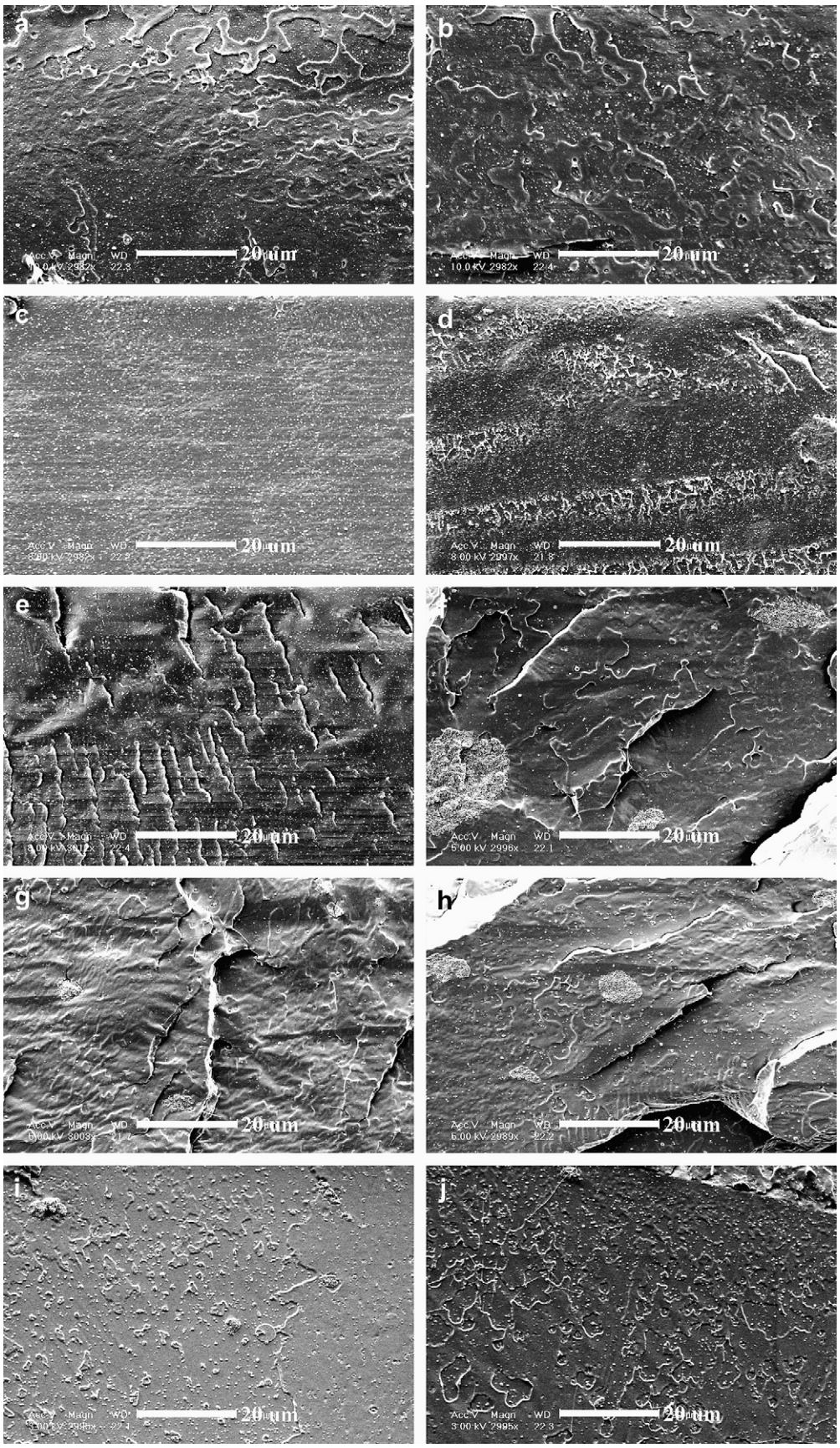

Fig. 8. SEM images of PLLA composites prepared via melt compounding under different screw rotation speed (a–e) PLLA/MWNT (f–j) PLLA/MWNT-*g*-POSS. The content of the MWNTs was 1% by weight. (a, f) 100 rpm, (b, g) 500 rpm, (c, h) 1000 rpm, (d, i) 1500 rpm, (e, j) 2000 rpm.

and the resulting SEM images are demonstrated in Fig. 7. The bright regions in the SEM images are attributed to MWNTs as a result of their high electrical conductivity. It is unambiguous from Fig. 7 that the MWNT-*g*-POSS (b) is homogeneously dispersed in the PLLA matrix without any aggregation while obvious aggregation is clearly observed in the PLLA/MWNT (a) composite.

Fig. 8 reveals the dispersion of MWNTs in the PLLA matrix during the melt compounding in which the different screw rotation speeds, namely from 100 to 2000 rpm, were selected. For the polymer composites with the functionalized additives, such as carbon nanotube and clay, the mixing time and shear force are the key factor controlling the morphological structure [45]. Applying a shear force should break up the primary particles and increase the uniformity. The homogeneous dispersion of additives in the polymer matrix is one of the most important requisites for the mechanical strength reinforcement because inhomogeneities normally lead to structural defects in the composite materials.

The SEM micrograph in Fig. 8a–e reveals a homogeneous dispersion of MWNTs throughout the PLLA/MWNT-*g*-POSS composites without aggregation or tactoid formation, which is indicative of a fully exfoliated structure of the PLLA/MWNT-*g*-POSS composite when the compounding was carried out at any rotation speed. In contrast, as shown in Fig. 8f–j, the dispersion of MWNTs is significantly depended on the screw rotation speed of the extruder. Aggregates are clearly observed in the PLLA/MWNT composites under low shearing, which means rotation speed is lower than 1500 rpm. At the same MWNT loading, composites with poor nanotube dispersion have discrete nanotube-rich domains rather than a nanotube network, such that the polymer chains flow independent of the nanotubes, and their motion is similar to that of pure PLLA. The dispersion of PLLA/MWNT becomes better when the rotation speed of extruder is higher than 1500 rpm.

DSC was employed to evaluate the effect of MWNTs on the phase transition behavior of PLLA. The glass transition temperature (T_g) of the hybrid composites is associated with a cooperative motion of long-chain segments, which may be hindered by the MWNT [46]. Therefore, as expected, both PLLA/MWNT and PLLA/MWNT-*g*-POSS composites recorded higher glass transition temperatures than pure PLLA as shown in Fig. 9 and Table 1. It was also found that the enhancement in T_g for PLLA/MWNT-*g*-POSS composite was more significant than that for PLLA/MWNT composite. It may be suggested that the higher enhancement in T_g for PLLA/MWNT-*g*-POSS composites is due to the strong interaction between the alkyl chains in POSS and the PLLA chains, and is able to hinder the motion of the polymer chains. Fig. 9 also shows that the melting temperature (T_m) of PLLA/MWNT-*g*-POSS composite decreased comparing with the pure PLLA. The marked decrease in T_m of PLLA/MWNT-*g*-POSS composite is probably the result of the CNTs nucleating and speeding up polymer crystallization in the polymer/CNT composites. Resultant imperfect polymer crystals in the composites will melt at a lower temperature than the control polymer.

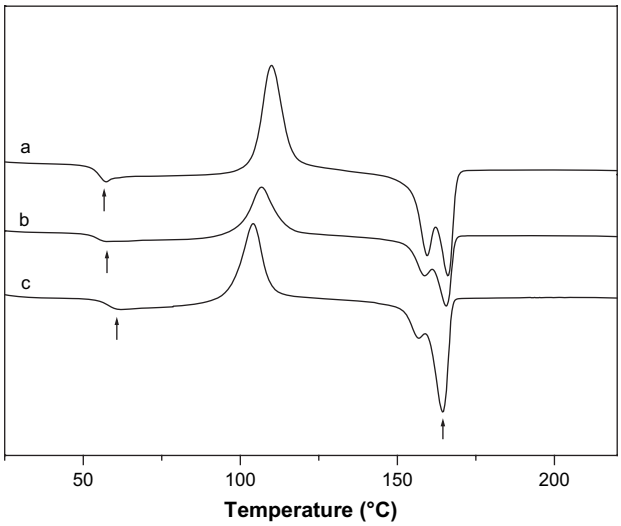

Fig. 9. DSC heating thermograms of (a) PLLA, (b) PLLA/MWNT and (c) PLLA/MWNT-*g*-POSS composites processing at 190 °C for 4 min under 1000 rpm. The content of the MWNTs was 1% by weight.

The Halpin–Tsai equation has been used successfully to predict the modulus of polymer/carbon nanotube composites [47,48]. Considering the random distribution of carbon nanotubes in the polymer matrix, the modified Halpin–Tsai equation is written as [49,50]:

$$E_C = \left[\frac{3}{8}\frac{1+2(l_{CNT}/D_{CNT})\eta_L V_{CNT}}{1-\eta_L V_{CNT}} + \frac{5}{8}\frac{1+2\eta_T V_{CNT}}{1-\eta_T V_{CNT}}\right]E_P \quad (1)$$

$$\eta_L = \frac{E_{CNT}/E_P - 1}{E_{CNT}/E_P + 2l_{CNT}/D_{CNT}} \quad (2)$$

$$\eta_T = \frac{E_{CNT}/E_P - 1}{E_{CNT}/E_P + 2} \quad (3)$$

where E_C, E_{CNT}, and E_P are the tensile modulus of the composite, nanotube, and polymer matrix, respectively. l_{CNT}, D_{CNT}, and V_{CNT} are the length, diameter, and volume fraction of the nanotubes in the composite, respectively. Aspect ratio (l_{CNT}/D_{CNT}) of the reinforcing nanotubes can be estimated if E_C, E_{CNT}, E_P, and V_{CNT} are known.

The modulus of the PLLA/MWNT-*g*-POSS composite (E_C) is plotted as a function of the MWNT-*g*-POSS loading in Fig. 10, setting the density of MWNT to be $\rho = 2.1$ g/cm^3. The average length, l_{CNT}, and diameter of the MWNT, D_{CNT}, were taken to be $l_{CNT} = 2.0$ μm and $D_{CNT} = 20$ nm. The value of E_{CNT} was assumed to be 1280 GPa.

Table 1
Glass transition temperature (T_g) and melt temperature (T_m) of PLLA, PLLA/MWNT, and PLLA/MWNT-*g*-POSS composites

Samples	T_g (°C)	T_m (°C)
PLLA	57.2	166.1
PLLA/MWNT	57.8	165.7
PLLA/MWNT-*g*-POSS	60.1	164.2

The content of the MWNTs is 1% by weight and the rotation speed is 1000 rpm.

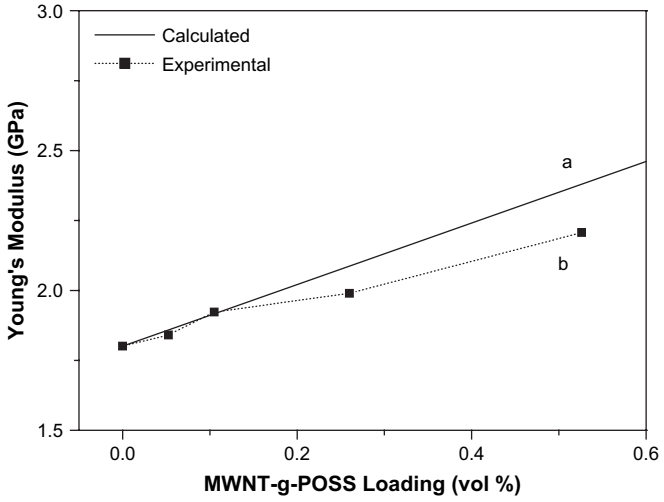

Fig. 10. Young's modulus calculated from the Halpin–Tsai equation under the assumptions: (a) MWN-*g*-POSS randomly distributed as a three dimension network in the composites, and (b) experimental values of the Young's modulus.

Fig. 10 shows that the experimentally measured Young's modulus of the composite which is close to the theoretically predicted values under the assumption that the MWNTs are randomly dispersed in the composites. This indicates that the MWNT-*g*-POSSs are dispersed isotropically in the composites. This is presumably due to the fact that the strong interaction between MWNT-*g*-POSS and PLLA chains, and the high melt viscosity of the composite hindered the orientation of the MWNT-*g*-POSSs in the matrix [51].

The tensile strength of the composite can be estimated as [52]:

$$\sigma_C = \sigma_{CNT} V_{CNT} + \sigma_P V_P \quad (4)$$

where σ_C, σ_{CNT}, and σ_P are the tensile strength of the composite, carbon nanotube, and polymer matrix, respectively. The results are summarized in Fig. 11. It is evident that the experimentally measured tensile strength fit very well with the theoretically

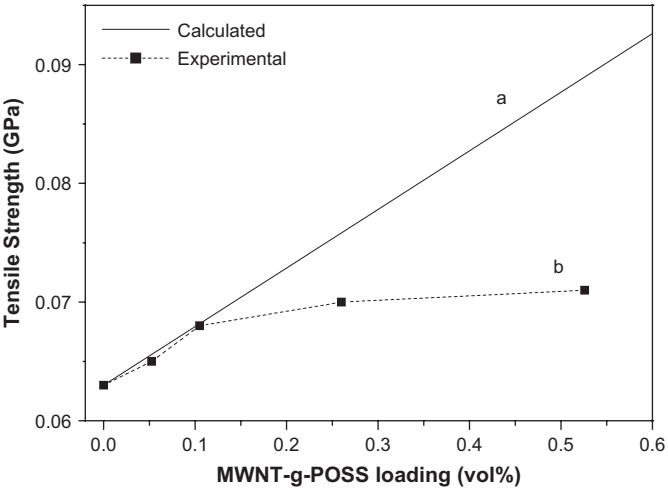

Fig. 11. Tensile strength as a function of MWNT-*g*-POSS loading: (a) calculated using Eq. (4), and (b) experimental.

estimated value at low MWNT-*g*-POSS loading, while the lower experimental value is obtained at high MWNT-*g*-POSS loading, indicating that the interfacial interaction is more effective in strengthening the material at low MWNT-*g*-POSS loading than at high MWNT-*g*-POSS loading.

4. Conclusions

MWNT was functionalized successfully with aminopropylisooctyl-POSS by reacting the amine group in POSS with the MWNT functionalized with –COCl groups, which was prepared by treating the purified MWNT with HNO_3 followed by $SOCl_2$. The retention of POSS even after extensive washing with a good solvent for the polymer was evidenced by the FTIR, Raman spectroscopy, and energy-filtering TEM. The TGA observations indicated the amount of the grafted POSS. The resulting MWNT-*g*-POSS dispersed in PLLA matrix very uniformly through either a solvent casting method or a simple melt compounding, which endows them with enhanced mechanical properties. Microscopic observations revealed that a more uniform and fine dispersion of MWNTs were achieved throughout the PLLA matrix after the functionalization due to the stronger interfacial adhesion between the nanotubes and the matrix.

Acknowledgment

G.X.C. would like to thank the Japan Society for the Promotion of Science (JSPS) for providing the fellowship and Grant-in-Aid ZCA33923D to do this research at National Institute of Advanced Industrial Science and Technology (AIST).

References

[1] Calvert P. Nature 1999;399:210.
[2] Salvetat JP, Briggs GAD, Bonard JM, Basca RR, Kulik AJ, Stockli T, et al. Phys Rev Lett 1999;82:944.
[3] Yu MF, Files BS, Arepalli S, Ruoff RS. Phys Rev Lett 2000;84:5552.
[4] Ajayan PM, Schadler LS, Giannaris C, Rubio A. Adv Mater 2000;12:750.
[5] Barrera EV. J Miner Met Mater Soc 2000;52A:38.
[6] McCarthy B, Coleman JN, Czerw R, Dalton AB, Panhuis MIH, Maiti A, et al. J Phys Chem B 2002;106:2210.
[7] Terrones M. Annu Rev Mater Res 2003;33:419.
[8] Satishkumar BC, Govindaraj A, Mofokeng J, Subbanna GN, Rao CNR. J Phys D: Appl Phys 1996;29:4925.
[9] Kuznetsova A, Mawhinney DB, Naumenko V, Yates Jr JT, Liu J, Smalley RE. Chem Phys Lett 2000;321:292.
[10] Ebbsen TW, Hiura H, Bischer ME. Adv Mater 1996;8:155.
[11] Jang J, Bae J, Yoon SH. J Mater Chem 2003;13:676.
[12] Mitchell CA, Bahr JL, Arepalli S, Tour JM, Krishnamoorti R. Macromolecules 2002;35:8825.
[13] Lin Y, Hill DE, Bentley J, Allard LF, Sun YP. J Phys Chem B 2003;107:10453.
[14] Chen J, Hamon MA, Hu H, Chen YS, Rao AM, Eklund PC, et al. Science 1998;282:95.
[15] Sun YP, Fu KF, Lin Y, Huang WJ. Acc Chem Res 2002;35:1096.
[16] Qin S, Qin D, Ford WT, Resasco DE, Herrera JE. J Am Chem Soc 2004;126:170.
[17] Niyogi S, Hamon MA, Hu H, Zhao B, Bhowmik P, Sen R, et al. Acc Chem Res 2002;35:1105.

[18] Raravikar NR, Schadler LS, Vijayaraghavan A, Zhao Y, Wei B, Ajayan PM. Chem Mater 2005;17:974.
[19] Lin Y, Zhou B, Fernando KAS, Liu P, Allard LF, Sun YP. Macromolecules 2003;36:7199.
[20] Hill DE, Lin Y, Rao AM, Allard LF, Sun YP. Macromolecules 2002;35:9466.
[21] Chen J, Rao AM, Lyuksyutov S, Itkis ME, Hamon MA, Hu H, et al. J Phys Chem B 2001;105:2525.
[22] Riggs JE, Guo Z, Carroll DL, Sun YP. J Am Chem Soc 2000;122:5879.
[23] Eitan A, Jiang K, Dukes D, Andrews R, Schadler LS. Chem Mater 2003;15:3198.
[24] Qin S, Qin D, Ford WT, Herrera JE, Resasco DE, Bachilo SM, et al. Macromolecules 2004;37:3965.
[25] Handge UA, Potschke P. Rheol Acta 2007;46:889.
[26] Huang YY, Ahir SV, Terentjev EM. Phys Rev B 2006;73:125422.
[27] Lichtenhan JD, Otonari YA, Carr MJ. Macromolecules 1995;28:8435.
[28] Haddad TS, Lichtenhan JD. J Inorg Organomet Polym 1995;5:237.
[29] Lichtenhan JD. Comments Inorg Chem 1995;17:115.
[30] Mantz RA, Jones PF, Chaffee KP, Lichtenhan JD, Gilman JW, Ismail IMK, et al. Chem Mater 1996;8:1250.
[31] Haddad TS, Lichtenhan JD. Macromolecules 1996;29:7302.
[32] Gilman JW, Schlitzer DS, Lichtenhan JD. J Appl Polym Sci 1996;60:591.
[33] Romo-Uribe A, Mather PT, Haddad TS, Lichtenhan JD. J Polym Sci Part B Polym Phys 1998;36:1857.
[34] Zhang C, Laine RM. J Organomet Chem 1996;521:199.
[35] Zheng S, Feher FJ, Xiao J, Jin R-Z. Polymer nanocomposites. In: Symposium proceeding series, vol. 733E. Warrendale, PA: Materials Research Society; 2002.
[36] Feher FJ. Book of Abstracts, 217th ACS National Meeting, Anaheim, CA, March 21–25, INOR; 1999.
[37] Feher FJ, Wyndham KD, Soulivong D, Nguyen F. J Chem Soc Dalton Trans 1999:1491.
[38] Chen GX, Li YJ, Shimizu H. Carbon 2007;45:2327.
[39] Horiuchi S, Yin D, Ougizawa T. Macromol Chem Phys 2005;206:725.
[40] Rao AM, Jorio A, Pimenta MA, Dantas MSS, Dresselhaus G, Dresselhaus MS. Phys Rev Lett 2000;84:1820.
[41] Jorio A, Pimenta MA, Souza Filho AG, Saito R, Dresselhaus G, Dresselhaus MS. New J Phys 2003;5:139.1.
[42] Wu HX, Tong R, Qiu XQ, Yang HF, Lin YH, Cai RF, et al. Carbon 2007;45:152.
[43] Wu HX, Qiu XQ, Cao WM, Lin YH, Cai RF, Qian SX. Carbon 2007;45:2866.
[44] Chen GX, Kim HS, Park BH, Yoon JS. J Phys Chem B 2005;109:22237.
[45] Das NC, Chaki TK, Khastgir D. Carbon 2002;40:807.
[46] Wu CS, Liao HT. Polymer 2007;45:4449.
[47] Qian D, Dickey EC, Andrews R, Rantell T. Appl Phys Lett 2000;76:2868.
[48] Cadek M, Coleman JN, Barron V, Hedicke K, Blau WJ. Appl Phys Lett 2002;81:5123.
[49] Mallick PK. Fiber-reinforced composites. New York: Marcel Dekker; 1993. p. 91–130.
[50] Zhang X, Liu T, Sreekumar TV, Kumar S, Moore VC, Hauge RH, et al. Nano Lett 2003;9:1285.
[51] Gao J, Itkis ME, Yu A, Bekyarova E, Zhao B, Haddon RC. J Am Chem Soc 2005;127:3847.
[52] Agarwal BD, Broutman LG. Analysis and performance of fiber composites. New York: Wiley; 1980.